JACS
JOURNAL OF THE AMERICAN CHEMICAL SOCIETY
Article
pubs.acs.org/JACS

Organic Solid Solution Composed of Two Structurally Similar Porphyrins for Organic Solar Cells

Yonggang Zhen,[†,‡,∥] Hideyuki Tanaka,*[,†,∥] Koji Harano,[†] Satoshi Okada,[†] Yutaka Matsuo,*[,†] and Eiichi Nakamura*[,†,§]

[†]Department of Chemistry, The University of Tokyo, 7-3-1 Hongo, Bunkyo-ku, Tokyo, 113-0033, Japan

[‡]Beijing National Laboratory for Molecular Sciences, Key Laboratory of Organic Solids, Institute of Chemistry, Chinese Academy of Sciences, Beijing 100190, China

[§]CREST, JST, 7-3-1 Hongo, Bunkyo-ku, Tokyo 113-0033, Japan

Supporting Information

ABSTRACT: A solid solution of a 75:25 mixture of tetrabenzoporphyrin (BP) and dichloroacenaphtho[*q*]-tribenzo[*b*,*g*,*l*]porphyrin (CABP) forms when they are generated in a matrix of (dimethyl(*o*-anisyl)silylmethyl)-(dimethylphenylsilylmethyl)[60]fullerene. This solid solution provides structural and optoelectronic properties entirely different from those of either pristine compounds or a mixture at other blending ratios. The use of this BP:CABP solid solution for organic solar cell (OSC) devices resulted in a power conversion efficiency (PCE) value higher by 16 and 300% than the PCE values obtained for the devices using the single donor BP and CABP, respectively, in a planar heterojunction architecture. This increase originates largely from the increase in short circuit current density, and hence by enhanced charge carrier separation at the donor/acceptor interface, which was probably caused by suitable energy level for the solid solution state, where electronic coupling between the two porphyrins occurred. The results suggest that physical and chemical modulation in solid solution is beneficial as an operationally simple method to enhance OSC performance.

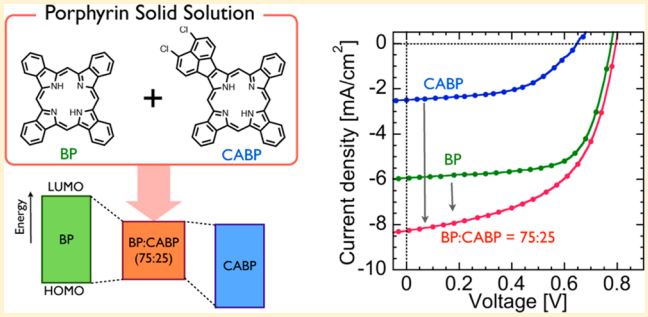

INTRODUCTION

Solid solution is common for minerals and inorganic solids but not for organic solids. This article reports on the use of an organic solid solution of a two structurally similar photoactive donor (D) molecules for an organic solar cell (OSC) to be combined with an electron acceptor (A) for a ternary blend active layer. Depending on the ratio of the two donors and the device fabrication method, the solid solution can made in a form of either bulk-heterojunction (BHJ) or planar hetero-junction (PHJ), and its properties are amenable to detailed study by a variety of physical method, providing detailed information on the function of a ternary blend active layer that have not been available for the recent related examples.[1−4] While most of the ternary blend OSCs operates on a parallel-linkage mechanism where absorbing materials individually contribute to photocurrent generation,[5,6] Thompson et al. recently proposed a "molecular alloy" model where two donors or acceptors are electronically coupled with each other and change the open-circuit voltage (V_{OC}).[7−11] Here however the physicochemical properties to molecular alloy and their relationship to the device performance have yet remained to be probed. Here, we report on a photovoltaic device based on a ternary mixture of a silylmethyl[60]fullerene acceptor (dimethyl(*o*-anisyl)silylmethyl)(dimethylphenylsilylmethyl)-[60]fullerene (SIMEF2),[12−14] tetrabenzoporphyrin (BP)[15−19] and dichloroacenaphtho[*q*]tribenzo[*b*,*g*,*l*]porphyrin (CABP; Figure 1a). The two porphyrins are designed to be structurally related to each other so that they phase-separate in a heated matrix (180 °C) of SIMEF2 to form a solid solution that was characterized in full after removal of SIMEF2 by toluene washing. This solid solution results only when BP and CABP in a 75:25 ratio are formed in a heated matrix of SIMEF2 to produce a PHJ structure, which showed a good OSC performance. Thus, the power conversion efficiency (PCE) increased by 16 and 300% as compared with the single-donor devices using BP and CABP, respectively. The PCE increase was caused mainly by the increase in short circuit current density (J_{SC}), and hence by enhanced charge carrier generation at the donor/acceptor interface (D/A).

The new morphology observed for the 75:25 BP:CABP mixture showed an X-ray diffraction (XRD) pattern mainly due to the BP crystal lattice, indicating that CABP molecules are homogeneously dispersed in the BP crystal lattice. This blend is therefore best described as a solid solution of CABP in BP. The present finding was made possible by the high crystallinity of

Received: June 6, 2014
Published: January 27, 2015

DOI: 10.1021/ja513045a
J. Am. Chem. Soc. 2015, 137, 2247−2252

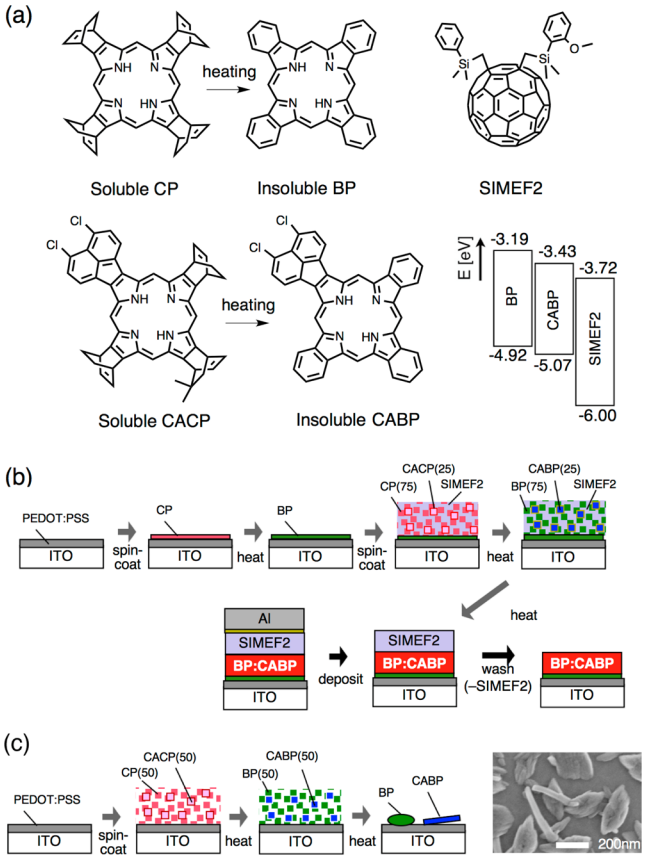

Figure 1. Design of the materials and devices. (a) Chemical structures, and energy level diagram of the molecules, and an illustration of the thermal conversion to BP and CABP. (b) Fabrication process to obtain the porphyrin solid solution films, which separate by heating a 75:25 CP/CACP mixture in a SIMEF2 matrix. The porphyrin blend film for the SEM observation was prepared by washing away SIMEF2 with toluene (right bottom), and OSCs were fabrication by the deposition of cathode buffer and aluminum electrodes (left bottom). (c) Thermolysis of a mixture and CP and CACP without SIMEF2 matrix and BP undercoating layer creating a mixture of BP and CABP crystals instead of their solid solution.

the two porphyrin molecules, which allowed us to remove the SIMEF2 matrix by toluene washing while keeping the porphyrin layer intact, and hence to study the morphology and physical properties of the solid solution. Such insolubility previously allowed us to find that half-molten morphology of SIMEF2 increases its contact to crystalline BP layer and hence increases the OSC performance.[13]

RESULTS AND DISCUSSION

Solid solutions are widely known for a mixture of two metals neighboring on the periodic table, but they have seldom been explored for organic solids, inter alia, in organic electronics research.[20,21] This is probably because of the difficulty in designing a crystalline mixture of different molecules, in which the minor component partially replaces the major component without changing the crystal lattice of the latter. To test the feasibility of preparing a porphyrin solid solution for a solution-processed small molecule OSC, we used the thermolysis of a soluble precursor (CP) in a matrix of SIMEF2 for in situ preparation of highly crystalline BP during device fabrication, as described previously.[12−15] We then designed a new soluble precursor (CACP; see Supporting Information for synthesis and crystal structure; the two additional methyl groups were introduced to a bicyclo moiety to increase the solubility of CACP, which is otherwise too insoluble) that thermally forms highly crystalline CABP with the loss of isobutane and ethylene molecules. CABP has three features that we consider to be useful for our study: structural similarity with BP, an acenaphthylene fragment that decreases the band gap, and two chlorine atoms that lower the highest occupied molecular orbital (HOMO) level which otherwise may not match well with that of BP. Fusion of an acenaphthylene group to a porphyrin skeleton is known to cause the largest red-shift in the absorption spectra among similar derivatizations using naphthalene, benzothiophene, or phenanthrene groups.[22,23]

By using two soluble donor precursors (CP and CACP) and the acceptor SIMEF2 serving as a matrix for the thermolysis of the precursors,[13] we first examined the morphology of the mixed porphyrin at different ratios (BP:CABP = 100:0 to 0:100). We found a new morphology at a 75:25 ratio where the donor phase looks entirely different from those formed at all other ratios. The blend films containing BP and CABP in a variety of ratios were fabricated according to the procedure shown in Figure 1b. A solution containing the two porphyrin precursors (30%) and SIMEF2 (70%) at the 2.0 wt % was spin-coated onto a BP undercoating layer and heated at 180 °C for 20 min. Upon heating, soluble CP and CACP in SIMEF2 generated crystalline BP and CABP within the SIMEF2 matrix, causing their deposition on the bottom BP layer. To examine morphology of the donor porphyrin blend, SIMEF2 was washed away using toluene, which does not dissolve BP and CABP crystals. It is this protocol of washing that makes the BP:CABP binary system unique among other OSC devices that are composed of donor and acceptor materials soluble in organic solvents.

A low-landing-voltage, high-resolution scanning electron microscope (SEM) is a state-of-the-art SEM that enables us to study the surface morphology of organic materials less than 1 nm resolution.[24,25] As illustrated by the top and dissection views in Figure 2, the 100:0 BP:CABP shows a nanocolumnar morphology of considerable regularity, which we reported previously (columns of ca. 20−30 nm diameter; Figure 2a).[12]

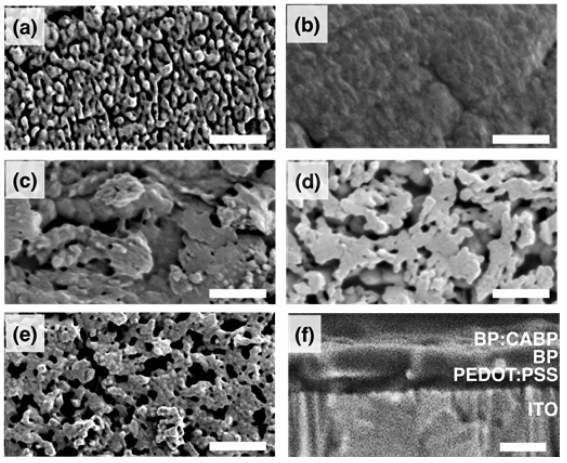

Figure 2. SEM images (a−f) for the blend of BP and CABP on the BP layer after removal of SIMEF2 by washing with toluene. Top view images at the BP:CABP blend ratios of 100:0 (a), 75:25 (b), 50:50 (c), 25:75 (d), and 0:100 (e), and a cross-sectional view of the 75:25 blend (f). Scale bar is 200 nm.

DOI: 10.1021/ja513045a
J. Am. Chem. Soc. 2015, 137, 2247−2252

The morphology of the CABP (0:100) is similar to that of the BP (100:0) but less ordered, consisting of a large number of small aggregates (Figure 2e).

In stark contrast, the 75:25 BP:CABP blend showed a very smooth surface reminiscent of a molten solid (Figure 2b) and the glass-like interior reminiscence of a solid solution (a dissection view in Figure 2f). The same morphology was also formed when we used a D/A ratio different from the 30/70 ratio used in the above experiments (see Supporting Information). The morphologies of the BP:CABP blends at the 50:50 and 25:75 ratios appear to be halfway between those of the 75:25 morphology and the pure BP or CABP morphology (Figure 2c,d).

Importantly, such characteristic nanoscale morphologies occurred only when the CP:CACP mixture was thermolyzed in the presence of SIMEF2 and the BP undercoating layer. Thus, thermolysis of a 50:50 mixture of CP and CACP on poly(3,4-ethylenedioxylenethiophene)−poly(styrenesulfonic) acid (PEDOT:PSS) without SIMEF2 and the BP undercoating layer produced a mixture of half micrometer-sized plates and needle crystals,[25] suggesting segregation during crystal growth of the two donor compounds in their binary blend (Figure 1c and Figure S7).

In addition to the SEM morphology analysis, in-plane thin-film XRD analysis of the BP:CABP mixed layer indicated the unique structure at the 75:25 ratio among the blends. Three noticeable changes occurred as the ratio was changed (Figure 3a and inset). First, the intensity of the peaks at 24.3° and 29.4° attributable to BP (113) and (114) (black triangle)[19] decreased as expected as the BP content was decreased from 100 to 25%. Second, the peak around 27.0° (green square; assigned to CABP by comparison with the powder XRD data, Figure S4) increased abruptly as the BP content was decreased from 25 to 0%, suggesting that the less symmetrical CABP molecules are less prone to form crystals than the highly symmetrical BP molecules. Third, a peak at 23.6° (orange circle) maximized at the 75:25 ratio suggesting that this peak represents a signature for the formation of a solid solution of CABP in the crystal lattice of BP (i.e., CABP molecules replacing some BP molecules in the crystal lattice of BP).

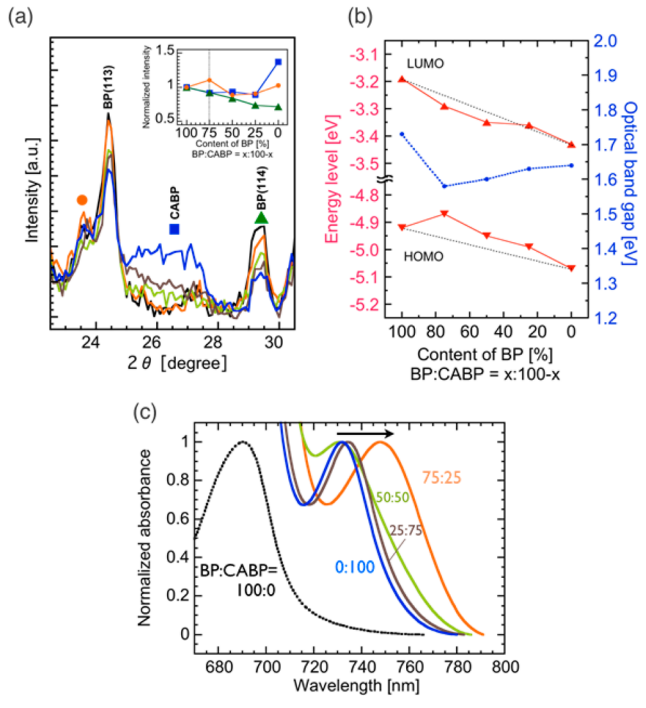

Figure 3. (a) Thin-film XRD patterns of the BP:CABP blend film at the ratios of 100:0 (black), 75:25 (orange), 50:50 (green), 25:75 (brown), and 0:100 (blue) coated on the BP undercoating layer. The inset shows the normalized XRD intensity at 23.6° (orange circle), 27.0° (blue square), and 29.4° (green triangle). (b) The HOMO and LUMO levels and optical band gap of the BP:CABP film at the different blend ratios. (c) Absorption spectra of the BP:CABP blend film at ratios of 100:0 (black), 75:25 (orange), 50:50 (green), 25:75 (brown), and 0:100 (blue) coated on the BP undercoating layer.

To identify the electronic energy level of the BP:CABP blend film, we next carried out a photoemission yield spectroscopy analysis for evaluating the HOMO level, and the measurement of absorption spectra. A nonlinear correlation between the BP content and the HOMO levels as well as with the optical band gap was observed (against a black dotted lines in Figure 3b). These measurements, as summarized in Figure 3b, revealed special characteristics of the 75:25 ratio. The HOMO levels of all blends, in particular that of the 75:25 blend (−4.87 eV), are markedly higher than the straight line connecting the HOMO levels of the 100:0 and the 0:100 devices (−4.92 eV (HOMO of BP) and −5.07 eV (HOMO of CABP)). A corresponding trend is found for the optical band gap, which minimizes at the 75:25 ratio (1.58 eV). In the data shown in Figure 3c, we found that the optical absorption at 729 nm originating from the Q-band of the CABP red-shifted toward 750 nm (at the 75:25 ratio) as the BP content is increased. The observed red shift can be attributed to intercalation of CABP into the BP matrix, where the acenaphthylene moiety of CABP enables J-aggregate with BP for red-shifted light absorption. The special morphological and electronic properties of the blend at the 75:25 ratio indicate that significant changes of the molecular assembly of the BP:CABP mixture occurs at this ratio.

The formation of new morphological and electronic features at the 75:25 ratio substantially influenced the OSC performance, giving the highest J_{SC} and the highest PCE that can be ascribed to effective charge carrier generation at the D/A interface. We first fabricated the device using a 30/70 donor/acceptor ratio while varying the BP:CABP ratio between 100:0 and 0:100, by depositing a buffer/Al electrode on top of the ternary blend BHJ. The OSC containing BP and CABP in a ratio of 75:25 showed the highest PCE, 2.7%, because of the increase in the J_{SC} (8.0 mA/cm^2) as show in Figure 4 and Table S1. Significant increase in J_{SC} from the BP cell (100:0) is mainly because of additional photocurrent around the 700−800 nm region, where the absorption of CABP certainly contributed to the photo carrier generation as confirmed in the external quantum efficiency (EQE) spectrum (Figure S8). Notably, only the device based on the 75:25 ratio formed a planar heterojunction structure (see SEM images in Figure 2) among tested devices with various BP:CABP ratios.

The foregoing paragraphs, in particular, the SEM images in Figure 2, indicated that the device made with a 75:25 ratio form a planar heterojunction (PHJ) structure (Figure 5a), while others form BHJ structures. This is because a mixture of BP and CABP phase-separate as a single solid solution phase from the SIMEF2 matrix. This discrepancy of the device structures makes it difficult to do fair comparison among the devices. We therefore prepared reference planar heterojunction (PHJ) devices for pure BP and CABP for comparison with the 75:25 BP:CABP PHJ device. The reference devices having a flat

DOI: 10.1021/ja513045a
J. Am. Chem. Soc. 2015, 137, 2247−2252

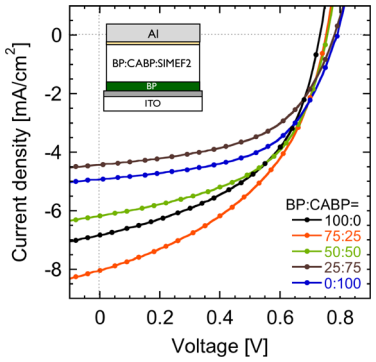

Figure 4. $J-V$ curves of ternary blend BHJ cells under AM 1.5 illumination at 100 mW/cm^2. The BP:CABP blend ratio are 100:0 (black), 75:25 (orange), 50:50 (green), 25:75 (brown), and 0:100 (blue). The 75:25 cell has a PHJ structure as described in the text. Inset shows the devices structure of ternary blend OSCs (ITO/PEDOT:PSS/BP/BP:CABP:SIMEF2/NBPhen/Al).

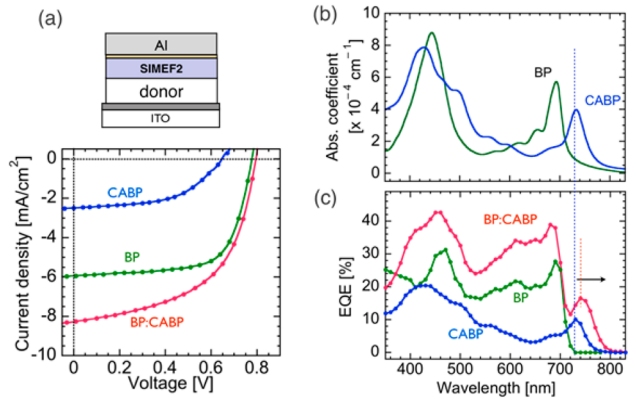

Figure 5. (a) Device structure of the PHJ cell, and current density vs voltage characteristics of the PHJ cell under 1 sun, AM 1.5 illumination. The BP (green), CABP (blue), and BP:CABP solid solution (red) was used as donor layer. (b) Absorption coefficient spectra of BP and CABP coated on quartz substrate. (c) External quantum efficiency spectra of the PHJ cell.

donor layer of pure BP and CABP were therefore fabricated by sequential spin coating of flat layers of the donor and SIMEF2 on ITO/PEDOT:PSS.

The device performance and photophysical properties for the three devices (100% BP, 72:25 BP:CABP, and 100% CABP) are summarized in Figure 5 and Table S2, and are discussed below. Each device was optimized separately by optimizing the thickness of the donor layer (Table S2). The best 75:25 BP:CABP showed a 3.6% PCE (Table S2), higher than the PHJ cells using 100% BP or CABP (3.1 or 0.9%, respectively), because of increase in J_{SC} (8.3–9.0 mA/cm^2). The device using only CABP donor showed a low J_{SC} of 2.5 mA/cm^2 and a large series resistance, which we may ascribe to poor charge transporting property caused by the less ordered packing structure.

To interpret the high J_{SC} value in the BP:CABP PHJ cell, we first examined the EQE spectrum and compared it with the BP and CABP cells. The BP:CABP cell showed a high EQE in the regions of 300–700 nm and 700–800 nm because of contributions from the absorption of both BP and CABP (Figure 5c). Notably, the EQE peak at 750 nm in the 75:25 cells was red-shifted by ca. 20 nm from the absorption peak of the CABP, as was also found for the absorption spectrum of the BP:CABP film (vide supra). This coincidence of the EQE and the absorption indicates that the molecular interaction between BP and CABP is responsible for the OSC performance. The most noticeable feature in the EQE spectrum is the remarkable enhancement at 350–700 nm, where both BP and CABP absorb strongly (Soret bands at 440 and 420 nm, respectively). We attribute this enhanced EQE to the improvement of internal quantum efficiency (IQE) rather than the absorption efficiency. This hypothesis was supported by the IQE spectra based on the reflectance measurement using an integrating sphere, which showed the effectiveness of the charge carrier generation in the BP:CABP cells. The IQE peaked at 460 nm to be 59% and at 740 nm to be 30% (Figure S9). The improved IQE in the solid solution may be explained by enhanced charge separation at the D/A interface. As shown in Figure 3b, the LUMO level of the BP:CABP solid solution formed at the 75:25 ratio is inbetween those of BP and CABP, causing an energy level offset, ΔLUMO of 0.43 eV at the D/A interface. This offset is favorable for the charge separation and improved carrier generation efficiency.[26]

A interesting property of the BP:CABP solid solution PHJ cell the V_{OC} value of 0.81 V, which is the highest among the BP/SIMEF-based solar cells thus far reported.[12−14,27] Even though the HOMO(donor)−LUMO(acceptor) energy level differences is the smallest for the solid solution cell among three cells (BP, BP:CABP, and CABP), the highest V_{OC} was obtained. This can be explained by suppressed recombination current J_{SO},[28] as summarized in Table 1. We consider that the

Table 1. Comparison of Calculated and Experimentally Obtained V_{OC} for the Optimized PHJ Cells Using Single BP, CABP, and BP:CABP Blend at the 75:25 Ratio

donor (thickness, nm)	HOMO [eV]	J_{SO} [mA/cm^2]	V_{OC} calc. [V]	V_{OC} exp. [V]
BP (30)	−4.92	0.3	0.78	0.77
BP:CABP (40)	−4.87	9.1×10^{-2}	0.80	0.81
CABP (20)	−5.07	3.2	0.66	0.65

CABP molecules intercalated in the BP crystal lattice induces partial disordering of the structure which decreases J_{SO} and hence increases V_{OC}. Overall, the results suggest that the organic solid solution formed by two molecules can be accounted as a good candidate for the semiconducting material rather than single component molecule because of its potential advantage to enhance both J_{SC} and V_{OC}.

CONCLUSION

In summary, we have fabricated a porphyrin solid solution thin film composed of a 75:25 mixture BP and CABP molecules, and investigated its photovoltaic performance in BHJ and PHJ architectures. The solid solution state formed at the 75:25 ratio of BP and CABP as they phase-separated from the SIMEF2/BP/CABP ternary mixture that showed unique planar morphology, high-lying HOMO level, narrower optical bandgap, and red-shifted light absorption toward the near-IR region as well as very small recombination current J_{SO}. We propose that these favorable properties originate from the formation of a solid solution of CABP in BP formed in the matrix of SIMEF2, which was characterized by its unique flat morphology, XRD, electronic properties and the OSC device performance. The available experimental data suggest that here CABP molecules are intercalated into the BP crystal lattice

DOI: 10.1021/ja513045a
J. Am. Chem. Soc. 2015, 137, 2247−2252

through $\pi-\pi$ interactions of the two structurally similar donor molecules. The PHJ device is effective for exciton dissociation, and hence better in J_{SC} and the overall performance than single donor reference devices using BP or CABP. In addition, this morphology contributes to suppress recombination current (J_{SO}) to improve V_{OC} (0.81 V), which is the highest value among reported BP/SIMEF-based OSCs. With this proof-of-principle study, molecular design for rational design of a solid solution and optimization of the physical parameters will be the next target of future studies. In addition, phase diagrams of multicomponent organic mixtures need to be studied in the future, as the studies on organic solid state lag behind those on inorganic solid state.

EXPERIMENTAL SECTION

SEM Observations. SEM observations were conducted on an FEI Magellan 400L equipped with AMETEK/EDAX Genesis APEX4 at an landing voltage of 200 V for top view and 1 kV for cross section view under a reduced pressure of 5×10^{-5} Pa. SEM samples were prepared following the device fabrication procedure described. SIMEF2 in the BHJ layer was washed out by spin-coating toluene twice at 1500 rpm for 30 s and drying at 70 °C under ambient conditions. The samples were then subjected to SEM observation without any metallic coatings.

Thin-Film XRD Analysis. The thin-film XRD analysis was performed on a Rigaku SmartLab X-ray diffractometer. The measurement employed focused Cu Kα radiation at 9 kW (45 kV, 200 mA) power using a 0.1° 2θ step scan over the range 2.0−50.0°.

Fabrication of OSC Devices. The devices were fabricated according to the following typical procedure. An indium tin oxide (ITO) layer on the glass substrate was 145 nm thick with a sheet resistance of 8 Ω/square. The surface roughness, R_a, was 0.7 nm and the R_{max} was 8.1 nm. Prior to the formation of the buffer layer, the patterned ITO glass was ultrasonically cleaned using a surfactant, rinsed with water, and then finally given UV−ozone treatment. A conducting PEDOT:PSS (Baytron AI4083) layer was formed on the ITO substrate by spin coating an aqueous dispersion to obtain a smooth 30 nm-thick film. The PEDOT:PSS-coated substrate was dried in air for 10 min at 120 °C, then dried in a nitrogen glovebox for 3 min at 180 °C prior to use. A BP layer was formed on the PEDOT:PSS layer by spin coating (1500 rpm) a precursor solution that contained 0.5 wt % of CP in a chloroform−chlorobenzene mixture (1:2 ratio). Thermal conversion was carried out at 180 °C for 20 min. The thickness of the crystallized BP p-layer was 25 nm. On top of the BP layer, the ternary blend BHJ layer was deposited by spin coating (1500 rpm) a mixture of CP, CACP, and a SIMEF2 (0.3 wt % for CP:CACP blend donor, 0.7 wt % for SIMEF2) in a 1,2-dichloroethane−chlorobenzene mixture (2:1 ratio). The ternary blend BHJ layer was heated at 180 °C for 20 min. After this, the device substrate was transferred from the glovebox to the vacuum chamber without exposure to air. The evaporation of a 2,9-bis(naphthalen-2-yl)-4,7-diphenyl-1,10-phenanthroline (NBPhen) buffer layer was carried out at a pressure of ca. 2×10^{-4} Pa. The deposition rate was typically 0.1 nm/s. After the deposition of the NBPhen layer (6−8 nm), the top electrode (Al, 80 nm) was deposited with a metal shadow mask, which defined a 2 mm stripe pattern perpendicular to the ITO stripe. Finally, the fabricated OSC was encapsulated with backing glass using a UV-curable resin under nitrogen atmosphere.

Fabrication of OSC Devices with the Planar Heterojunction. The PHJ devices as reference to the 75:25 CABP:BP PHJ device are illustrated by the following procedure: The PEDOT:PSS-coated ITO glass substrate was prepared as described above. A precursor solution that contains 0.5 wt % of CP (or CACP) in a $CHCl_3$/chlorobenzene mixture (1:2) or 0.4 wt % of CACP in a 1,2-dichloroethane/chlorobenzene mixture (2:1) was then spin-coated (1500 rpm) onto the PEDOT:PSS layer. Thermal conversion was carried out at 180 °C for 20 min to obtain a layer of BP (or CABP). SIMEF2 (0.7 wt %) was spin-coated (3000 rpm) from a solution of toluene to obtain the acceptor layer. After drying this film for 10 min at 120 °C, the device substrate was transferred from a glovebox into the vacuum chamber without exposure to air. NBphen and Al electrode were deposited as described above to obtain the PHJ devices.

Evaluation of OSC Devices. The encapsulated OSCs were subjected to $J-V$ measurements under both dark and irradiated conditions. Current−voltage sweeps were taken with a Keithley 2400 source measurement unit controlled by a computer. The light source used to determine the PCE was an AM1.5G solar simulator system (Sumitomo Heavy Industries Advanced Machinery) with an intensity of 100 mW/cm^2. For the EQE measurement, a constant power mode was employed using monochromatized photons from halogen or xenon lamps. EQE and IQE measurements were determined using an Oriel IQE 200 (Newport).

ASSOCIATED CONTENT

Supporting Information

Synthetic procedures, method for fabrication of the OSC devices and SEM images, details of OSC data, and crystallographic data (CIF). This material is available free of charge via the Internet at http://pubs.acs.org.

AUTHOR INFORMATION

Corresponding Authors

tanakah3@chem.s.u-tokyo.ac.jp
matsuo@chem.s.u-tokyo.ac.jp
nakamura@chem.s.u-tokyo.ac.jp

Author Contributions

‖Y.Z. and H.T. made equal contributions.

Notes

The authors declare no competing financial interest.

ACKNOWLEDGMENTS

We thank MEXT for financial support [KAKENHI Specially Promoted Research Grant 22000008 to E.N., and Grant-in-Aid for Challenging Exploratory Research 26620203 to H.T.]. This study was partially supported by the Strategic Promotion of Innovative Research and Development from the Japan Science and Technology Agency (to E.N.).

REFERENCES

(1) Yang, L.; Yan, L.; You, W. *J. Phys. Chem. Lett.* **2013**, *4*, 1802.
(2) Chen, Y.-C.; Hsu, C.-Y.; Lin, R. Y.-Y.; Ho, K.-C.; Lin, J. T. *ChemSusChem* **2013**, *6*, 20.
(3) Ameri, T.; Khoram, P.; Min, J.; Brabec, C. J. *Adv. Mater.* **2013**, *25*, 4245.
(4) Varotto, A.; Nam, C.-Y.; Radivojevic, I.; Tomé, J. P. C.; Cavaleiro, J. A. S.; Black, C. T.; Drain, C. M. *J. Am. Chem. Soc.* **2010**, *132*, 2552.
(5) Ojala, A.; Bürckstümmer, H.; Stolte, M.; Sens, R.; Reichelt, H.; Erk, P.; Hwang, J.; Hertel, D.; Meerholz, K.; Würthner, F. *Adv. Mater.* **2011**, *23*, 5398.
(6) Yang, L.; Zhou, H.; Price, S. C.; You, W. *J. Am. Chem. Soc.* **2012**, *134*, 5432.
(7) Khlyabich, P. P.; Burkhart, B.; Thompson, B. C. *J. Am. Chem. Soc.* **2011**, *133*, 14534.
(8) Khlyabich, P. P.; Burkhart, B.; Thompson, B. C. *J. Am. Chem. Soc.* **2012**, *134*, 9074.
(9) Street, R. A.; Davies, D.; Khlyabich, P. P.; Burkhart, B.; Thompson, B. C. *J. Am. Chem. Soc.* **2013**, *135*, 986.
(10) Khlyabich, P. P.; Rudenko, A. E.; Street, R. A.; Thompson, B. C. *ACS Appl. Mater. Interfaces* **2014**, *6*, 9913.
(11) Street, R. A.; Khlyabich, P. P.; Rudenko, A. E.; Thompson, B. C. *J. Phys. Chem. C* **2014**, *118*, 26569.
(12) Matsuo, Y.; Sato, Y.; Niinomi, T.; Soga, I.; Tanaka, H.; Nakamura, E. *J. Am. Chem. Soc.* **2009**, *131*, 16048.
(13) Tanaka, H.; Abe, Y.; Matsuo, Y.; Kawai, J.; Soga, I.; Sato, Y.; Nakamura, E. *Adv. Mater.* **2012**, *24*, 3521.

DOI: 10.1021/ja513045a
J. Am. Chem. Soc. 2015, 137, 2247−2252

(14) Matsuo, Y.; Oyama, H.; Soga, I.; Okamoto, T.; Tanaka, H.; Saeki, A.; Seki, S.; Nakamura, E. *Chem.—Asian J.* **2013**, *8*, 121.
(15) Aramaki, S.; Sakai, Y.; Ono, N. *Appl. Phys. Lett.* **2004**, *84*, 2085.
(16) Ku, S.-Y.; Liman, C. D.; Cochran, J. E.; Toney, M. F.; Chabinyc, M. L.; Hawker, C. J. *Adv. Mater.* **2011**, *23*, 2289.
(17) Guide, M.; Dang, X.-D.; Nguyen, T.-Q. *Adv. Mater.* **2011**, *23*, 2313.
(18) Noguchi, N.; Junwei, S.; Asatani, H.; Matsuoka, M. *Cryst. Growth Des.* **2010**, *10*, 1848.
(19) Aramaki, S.; Mizuguchi, J. *Acta Crystallogr., Sect. E: Struct. Rep. Online* **2003**, *59*, 1556.
(20) Shao, Y.; Yang, Y. *Adv. Funct. Mater.* **2005**, *15*, 1781.
(21) Liu, J.; Shi, Y.; Yang, Y. *Appl. Phys. Lett.* **2001**, *79*, 578.
(22) Yamada, H.; Okujima, T.; Ono, N. *Chem. Commun.* **2008**, 2957.
(23) Lash, T. D.; Chandrasekar, P. *J. Am. Chem. Soc.* **1996**, *118*, 8767.
(24) Harano, K.; Minami, K.; Noiri, E.; Okamoto, K.; Nakamura, E. *Chem. Commun.* **2013**, *49*, 3525.
(25) Harano, K.; Okada, S.; Furukawa, S.; Tanaka, H.; Nakamura, E. *J. Polym. Sci., Part B: Polym. Phys.* **2014**, *52*, 833.
(26) Peumans, P.; Forrest, S. R. *Chem. Phys. Lett.* **2004**, *398*, 27.
(27) Tanaka, H.; Andersson, L. M. *Appl. Phys. Lett.* **2014**, *104*, 043304.
(28) Perez, M. D.; Borek, C.; Forrest, S. R.; Thompson, M. E. *J. Am. Chem. Soc.* **2009**, *131*, 9281.

DOI: 10.1021/ja513045a
J. Am. Chem. Soc. 2015, 137, 2247−2252